INTERNATIONAL JOURNAL OF CLIMATOLOGY
Int. J. Climatol. **36**: 2942–2957 (2016)
Published online 9 November 2015 in Wiley Online Library
(wileyonlinelibrary.com) DOI: 10.1002/joc.4530

RMetS
Royal Meteorological Society

Observed variability of summer precipitation pattern and extreme events in East China associated with variations of the East Asian summer monsoon

Lei Wang,[a,b] Yun Qian,[b] Yaocun Zhang,[a]* Chun Zhao,[b] L. Ruby Leung,[b] Anning Huang[a] and Chuliang Xiao[c]

[a] *School of Atmospheric Sciences, Nanjing University, China*
[b] *Pacific Northwest National Laboratory, Richland, WA, USA*
[c] *Cooperative Institute for Limnology and Ecosystems Research, School of Natural Resources and Environment, University of Michigan, Ann Arbor, MI, USA*

ABSTRACT: This article presents a comprehensive analysis of interannual and interdecadal variations of summer precipitation and precipitation-related extreme events in East China associated with variations of the East Asian summer monsoon (EASM) from 1979 to 2012. A high-quality daily precipitation data set covering 2076 observational stations in China is analysed. Based on the precipitation pattern analysis using empirical orthogonal functions and the regime shift detection method, three sub-periods of 1979–1992 (period I), 1993–1999 (period II) and 2000–2012 (period III) are identified to be representative of the precipitation variability. Similar significant variability of the extreme precipitation indices is found across four sub-regions in eastern China. The spatial patterns of summer mean precipitation, the number of days with daily rainfall exceeding 95th percentile precipitation (R95p) and the maximum number of consecutive wet days (CWD) anomalies are consistent, but opposite to that of maximum consecutive dry days (CDD) anomalies to some extent during the three sub-periods. However, the spatial patterns of hydroclimatic intensity (HY-INT) are notably different from that of the other three extreme indices, but highly correlated to the dry events. The changes of precipitation anomaly patterns are accompanied by the change of the EASM regime and the abrupt shift of the position of the west Pacific subtropical high around 1992/1993 and 1999/2000, respectively, which influence the moisture transport and contributes to the precipitation anomalies. In addition, the EASM intensity is linked to sea surface temperature anomaly over the tropical Indian and Pacific Ocean through its effects on convective activity over the west Pacific that induces the cyclonic or anticyclonic anomaly over the South China and northwest Pacific.

KEY WORDS precipitation pattern; extreme event; East Asia; summer monsoon

Received 23 February 2015; Revised 5 August 2015; Accepted 15 September 2015

1. Introduction

Extreme precipitation, with the potential for serious consequences to the economy and life (e.g. Kunkel *et al.*, 1999; Changnon, 2003), has attracted increasing attention from the public and scientific community around the world (e.g. Alexander *et al.*, 2006; Moberg *et al.*, 2006; Piao *et al.*, 2010). Through changes in the atmospheric circulation and moisture content, climate change can lead to changes in both the mean and extreme precipitation (Trenberth *et al.*, 2003). Understanding the changing feature and formation mechanism of extreme precipitation, as well as its relationship with the atmospheric circulations, is critical for increasing confidence in projections of future changes in extreme precipitation by climate models.

As shown in the Fifth Assessment Report of the Intergovernmental Panel on Climate Change (IPCC-AR5), the changes in heavy (or 'extreme') precipitation events since 1951 exhibit strong regional differences. East China, located in East Asian monsoon region, is vulnerable to heavy precipitation (Huang *et al.*, 2007) that exhibits complex temporal and spatial variations (e.g. Qian and Lin, 2005; Zhai *et al.*, 2005; Qian and Leung, 2007; Yao *et al.*, 2008). This complicates investigations on the occurrence, changing characteristics and underlying mechanisms of extreme precipitation. Previous studies found important differences in the historical trends of extreme events over different time periods and regions in East China (e.g. Wang and Zhou, 2005; Zhai *et al.*, 2005; Qian *et al.*, 2009; Zhang *et al.*, 2011). For instance, Zhai *et al.* (2005) showed an increasing trend of annual extreme precipitation days in the middle Yangtze River valley during 1951–2000, while Qian and Lin (2005) found decreasing trends of annual maximum number of consecutive wet days (CWD) in the same region between 1961–1980 and 1981–2000. Wang and Zhou (2005) demonstrated that increasing trend of summer extreme precipitation days occurred mainly over the mid-lower Yangtze River Basin during 1961–2001, while a decreasing trend was found in North China and Sichuan Basin.

* Correspondence to: Y. Zhang, School of Atmospheric Sciences, Nanjing University, 163 Xianlin Ave, Nanjing 210023, China. E-mail: yczhang@nju.edu.cn

© 2015 Royal Meteorological Society

Overall, the long-term trend of extreme precipitation in East China is not significant due to the large interannual and interdecadal variability (Li *et al.*, 2012). In Northeast China, more annual heavy rainfall days are observed in the 1960s, 1980s and 1990s, but fewer in the 1970s and 2000s (Chen *et al.*, 2012). The significant decadal transitions in the frequency and intensity of annual heavy rainfall events (HRE) can also be detected in other regions of East China in the past 50 years. The annual heavy rainfall days over the Huai River basin experience significant decrease since 1960s, and increase after 1990s (Chen *et al.*, 2010). Other large river basins show their individual decadal characteristics during 1956–2008. The studies to date investigated the interannual and interdecadal variability of extreme precipitation changes in intensity, frequency and duration (Zhai *et al.*, 1999; Zhang *et al.*, 2008; Chen *et al.*, 2010, 2012). However, interannual and interdecadal variability of summer extreme events in East China associated with the variations of the East Asian summer monsoon (EASM) was not fully explored yet.

In this article, we focused on the interannual and interdecadal variations of summer extreme events associated with variations of the EASM. On a broader scale, East Asia has experienced four abrupt summer climate shifts in the mid-1960s, the late 1970s, and the early and late 1990s, respectively (e.g. Wang, 2001; Xue, 2001; Kwon *et al.*, 2007). The summer precipitation in East China responds differently to these abrupt changes in different regions. The first abrupt change is reflected by the decreased precipitation over North China after 1965. The second is the so-called 'flood in the south and drought in the north' trend that begins in the late 1970s in East China, i.e. flood near the Yangtze-Huai River Basin and drought in North China as well as South China (Hu, 1997; Lu, 1999, 2003; Wu and Wang, 2002; Yu *et al.*, 2004). The third climate shift is detected in South China with more precipitation in the early 1990s (Kwon *et al.*, 2007; Ding *et al.*, 2008). Following the fourth shift, more precipitation occurs in the Huang-Huai River Basin and less occurs in the Yangtze River valley after the late 1990s (Zhu *et al.*, 2010; Huang *et al.*, 2011a, 2011b). In addition, both annual and seasonal precipitation has high correlation with extreme precipitation in China (Wang and Yan, 2009; You *et al.*, 2011; Chen *et al.*, 2012). Therefore, based on the interannual and interdecadal variations of summer precipitation since 1970s and the relationship between mean and extreme precipitation, the systematical analysis of the variation characteristics of summer extreme events associated with the variations of the EASM is therefore important for understanding the regularity of extreme events. Moreover, a new measure of hydroclimatic intensity (HY-INT) proposed by Giorgi *et al.* (2011), describing the risk of extreme events, is adopted in East China for the first time. The analysis of HY-INT may give us some new understandings of the extreme events in East China. In addition, we attempt to provide the possible mechanisms for the interannual and interdecadal variations of mean and extreme precipitation changes. In this article, first we examine the interannual and interdecadal variations of summer precipitation in East China associated with the change of the EASM (Section 3.1). In Section 3.2, we investigate the extreme precipitation in different time periods and regions. We discuss the possible mechanisms of precipitation change in Section 3.3. Finally, the conclusions and discussion are presented in Section 4.

2. Data and methods

2.1. Data

The daily precipitation data at 2474 observational stations over China during 1979–2012 are used in this study. With the strict quality control by China Meteorological Information Center, this higher quality data set is more appropriate for detecting local changes of extreme events and generally shows higher precipitation intensity compared with former studies. We focus on analysis of summer precipitation and extreme events in June, July and August (JJA). To ensure accuracy of the statistics, data from stations with more than 5% missing days of observations in the summer of each year are not used. As a result, data from 2076 stations (Figure 2(a)) are used to provide precipitation observations for analysis.

We also employ the National Centers for Environmental Prediction/National Center for Atmospheric Research (NCEP/NCAR) reanalysis data set of monthly mean surface pressure, geopotential height, horizontal and vertical winds and specific humidity at a horizontal resolution of $2.5° \times 2.5°$ (Kalnay *et al.*, 1996). In order to get robust conclusion, other two reanalysis data sets are used in this study, including monthly 850 hPa winds from Modern Era Retrospective Analysis for Research and Applications (MERRA), with a horizontal resolution of $1/2° \times 2/3°$ (Rienecker *et al.*, 2011), and European Centre for Medium-Range Weather Forecasts (ECMWF) Interim Reanalysis (ERA-interim), with a horizontal resolution of $1.5° \times 1.5°$ (Dee *et al.*, 2011). Monthly mean sea surface temperature (SST) from Hadley Centre Sea Ice and Sea Surface Temperature (HadISST) (Rayner *et al.*, 2003) data set with a grid mesh of $1° \times 1°$ and outgoing longwave radiation (OLR) data obtained from National Oceanic and Atmospheric Administration (NOAA) (Liebmann and Smith, 1996) with $2.5° \times 2.5°$ horizontal resolution are also used.

2.2. Methods

To analyse extreme events quantitatively, four extreme indices are used in this study: number of days with daily rainfall exceeding 95th percentile precipitation (R95p), maximum number of CWD, maximum number of consecutive dry days (CDD) and HY-INT. We adopt the first three indices used by the CCl/CLIVAR Working Group on Climate Change Detection (Peterson *et al.*, 2001) to characterize summer extreme precipitation. The last index HY-INT defined by Giorgi *et al.* (2011) is a new measure of HY-INT, which integrates the extreme dry and/or wet events. From the definitions listed in Table 1, these

© 2015 Royal Meteorological Society

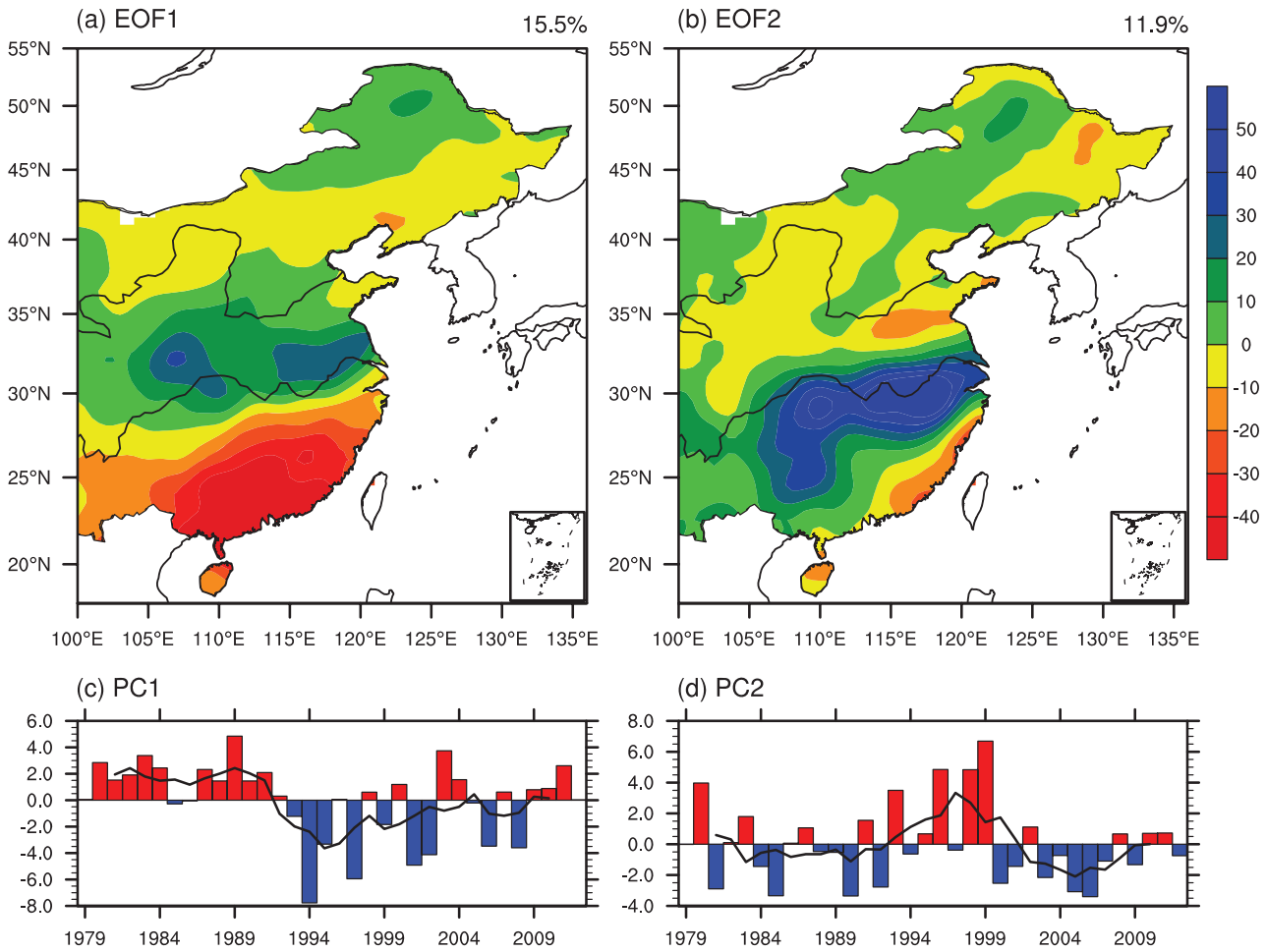

Figure 1. Spatial distribution (a, b) and PC time series (c, d) of the two leading EOFs of summer total precipitation in East China for the period 1979–2012. The solid line in (c) and (d) is the 9-year running mean.

four indices are divided into three categories: percentile, duration and ensemble index, which assess extreme events from the perspectives of occurrence frequency, persistent and risk of occurrence, respectively.

We follow the definition of seasonal percentile index in Sánchez *et al.* (2004). The percentile thresholds are calculated from the full time period, 1979–2012 ($34 \times 92 = 3128$ data samples at each station), and the climatological annual mean is produced for the same base period.

3. Results

3.1. Precipitation patterns in East China and the weakening EASM

The interdecadal variation of EASM has been examined by numerous previous studies with the conclusion that EASM has experienced two apparent interdecadal weakening in mid-1960s and late 1970s (Wang, 2001; Xue, 2001; Guo *et al.*, 2003; Huang *et al.*, 2004; Jiang and Wang, 2005). Accompanying the two interdecadal shifts of EASM, the climate in East China changes with drier in North China after 1965 and wetter in the Yangtze River Basin after the late 1970s (e.g. Hu, 1997; Wu and Wang, 2002; Lu, 2003; Yu *et al.*, 2004). These change patterns motivate a question of how the precipitation patterns and extreme events in East China change associated with the variations of EASM after 1979.

Sun and Wang (2014) suggested that the leading empirical orthogonal function (EOF) mode of precipitation in East China represents the dominating pattern of the interannual variability of precipitation. Xu *et al.* (2015) also used EOF analysis of the summer precipitation to confirm the representative years for the decadal variations of summer precipitation over China. So we address the question mentioned above using EOF to analyse the summer total precipitation in East China from 1979 to 2012. Figure 1 shows the spatial modes and time series of the first two leading EOF modes (EOF-1 and EOF-2). These two EOF modes together account for 27.4% of the total variance. Although the percentage variances explained by them are close, they are well separated from each other according to the criteria of North *et al.* (1982). The spatial mode of EOF-1 shows a meridional distribution with a 'negative–positive-negative' pattern; i.e. major positive precipitation anomalies are located in Central China and negative anomalies occur over South and North China. This pattern is quite similar to the EOF-1 described by

© 2015 Royal Meteorological Society

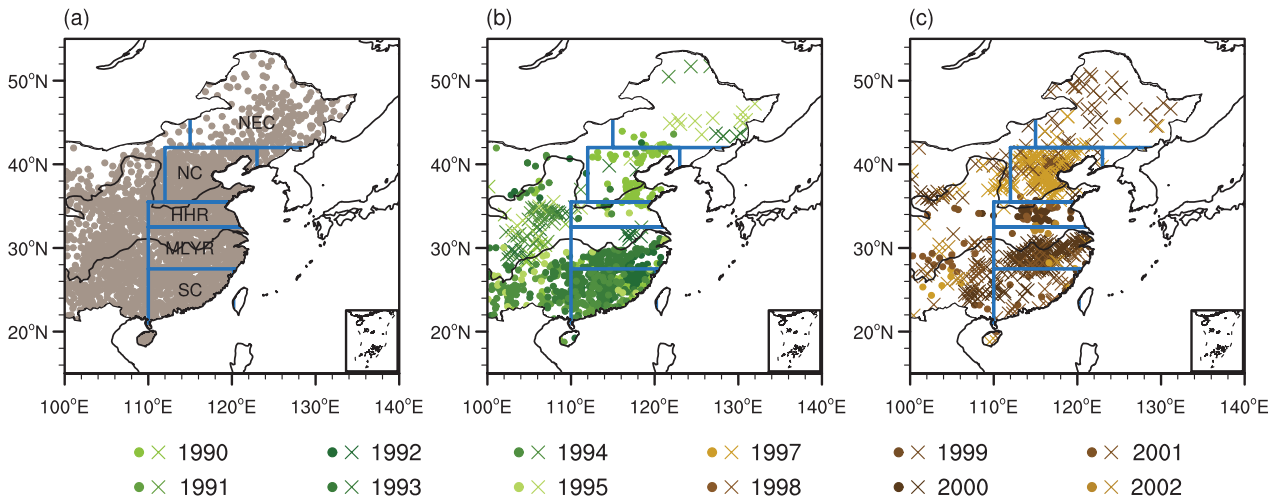

Figure 2. Location of 2076 weather stations (a), the regime shift detection method for shift years around 1992/1993 (b) and 1999/2000 (c). The shift stations with an increase (decrease) in precipitation shown with coloured dots (crosses). The regions with light blue lines in (a) indicate five sub-regions: NEC, NC, HHR, MLYR, SC used in this study.

Table 1. Summer extreme precipitation indices.

Index category	Precipitation indices	Definitions	Units
Percentile	R95p	Summer number of days when daily rainfall ($\geq$0.1 mm day^{-1}) > 95th percentile precipitation	Days
Duration	CWD	Summer maximum number of consecutive wet days ($\geq$1 mm day^{-1})	Days
	CDD	Summer maximum number of consecutive dry days (<1 mm day^{-1})	Days
Ensemble	HY-INT	HY-INT = INT × DSL	

Wet days, daily precipitation ≥ 1 mm (You *et al.*, 2011); dry days, daily precipitation < 1 mm; INT (wet event), the summer mean precipitation intensity during wet days; DSL (dry event), the summer mean number of consecutive dry days during each dry spell. Both INT and DSL are normalized by their minimum and maximum values, respectively.

Li and Leung (2013) and EOF-2 by Zhou and Yu (2005). The time series, or principle component (PC), of EOF-1 is also the same as those found in these previous studies, with marked interdecadal transition in 1992/1993 that indicates the occurrence of heavy precipitation over Central China during 1979–1992 and shift to South China during 1993–2012. The EOF-2 spatial pattern shows large precipitation anomaly over middle-lower Yangtze River Basin (MLYRB). Like EOF-PC1, EOF-PC2 also shows obvious interdecadal transition in 1999/2000. During the period of 1993–1999, heavy precipitation is mainly over the MLYRB, while it jumps to Huang-huai River Basin during the period of 2000–2012.

To confirm further the interannual and interdecadal transition of precipitation in East China, the sequential *T*-test analysis of regime shifts (Rodionov, 2004) is adopted. In this article, the cut-off regime length is set to 7 years, and the property level to 0.1. We detect the regime shift at individual stations. The location of the regime shift detection method for shift years around 1992/1993 and 1999/2000 is illustrated in Figure 2. Many stations over East China, including South China, Southwest China and North China, experience significant regime shifts towards increased precipitation around 1992/1993, while the shift stations with a decrease in precipitation are mainly over Sichuan Basin (Figure 2(b)). This significant anti-phase precipitation change around 1992/1993 between Sichuan Basin and South China is consistent with the spatial distribution of the first EOF mode. The regime shifts associated with the decreased precipitation around 1999/2000 could be found over Northeast China, North China, part of MLYRB and South China (Figure 2(c)), implying an abrupt change of precipitation in East China during these years.

Based on the two time series of EOF and analysis of regime shifts, we divide the entire time period into three sub-periods: 1979–1992 (period I), 1993–1999 (period II) and 2000–2012 (period III), which is similar to previous studies (Zhu *et al.*, 2010; Huang *et al.*, 2011a, 2011b, 2013). In the next section, the analysis will focus on the changes in precipitation anomaly patterns and extreme events during these three sub-periods.

3.2. Anomalies in precipitation patterns and extreme events

Figure 3 depicts the spatial anomalies of summer precipitation for the three sub-periods relative to the summer mean of 1979–2012. In period I (Figure 3(a)), the major rainbelt is oriented from Northeast China to Sichuan Basin in the

© 2015 Royal Meteorological Society

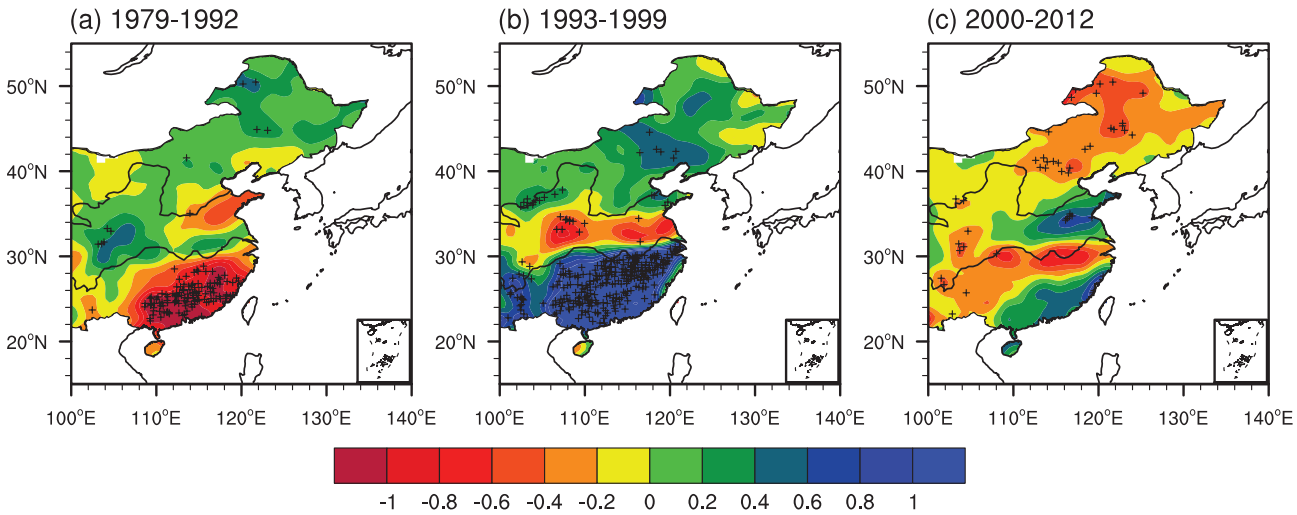

Figure 3. Anomalies of summer mean precipitation (mm day^{-1}) averaged for the three sub-periods: (a) 1979–1992, (b) 1993–1999 and (c) 2000–2012, relative to the 1979–2012 average. The black crosses indicate the mean precipitation exceeding the 90% significance level based on the Student's *t*-test.

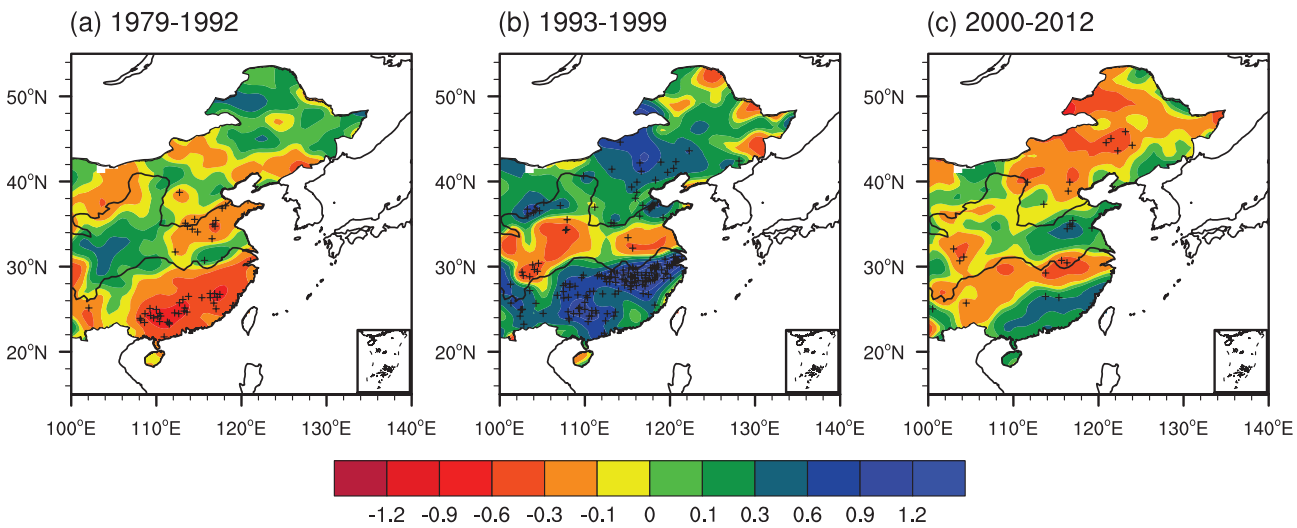

Figure 4. Anomalies of number of days with daily precipitation exceeding 95th percentile (R95p, days year^{-1}) during summer for the three sub-periods: (a) 1979–1992, (b) 1993–1999 and (c) 2000–2012, relative to the 1979–2012 average. The black crosses indicate the R95p exceeding the 90% significance level based on the Student's *t*-test.

northeast-southwest direction. Meanwhile, precipitation is enhanced over the Yangtze-Huai River Basin and reduced over the Huang-huai River Basin, South and most parts of Southwest China, respectively. The precipitation pattern in period I is consistent with the EOF results, showing wet conditions in the Sichuan Basin and dry conditions in South China. The pattern correlation coefficient between the precipitation pattern in period I and the mode of EOF-1 is up to −0.84.

In period II (Figure 3(b)), the distribution of the precipitation anomaly pattern is more meridional. Negative precipitation anomalies mainly occur in the central meridional belt of East China, sandwiched between significant positive anomalies to the north and south of the belt, i.e. precipitation increases since 1992 north of Yellow River and south of Yangtze River. This pattern is similar to the EOF-1 mode (pattern correlation coefficient = 0.69).

In period III (Figure 3(c)), a reverse pattern to period I is shown (pattern correlation coefficient = −0.64). Regions east of 103°E (i.e. Northeast China, Southwest China and the MLYRB) are relatively dry after 1999, while more precipitation occurs over Huang-huai River Basin and South China. The negative precipitation anomalies around MLYRB and Northeast China are associated with the large variation amplitude of PC2 during period III.

Figure 4 shows the spatial distributions of the R95p anomalies in the three sub-periods. Despite the larger spatial variability, the R95p anomaly pattern is consistent with the mean precipitation anomaly patterns shown in Figure 3. During the three sub-periods, high frequency of extreme precipitation is concentrated mostly in the same regions with positive precipitation anomalies. The pattern correlation coefficients between R95p and precipitation

© 2015 Royal Meteorological Society

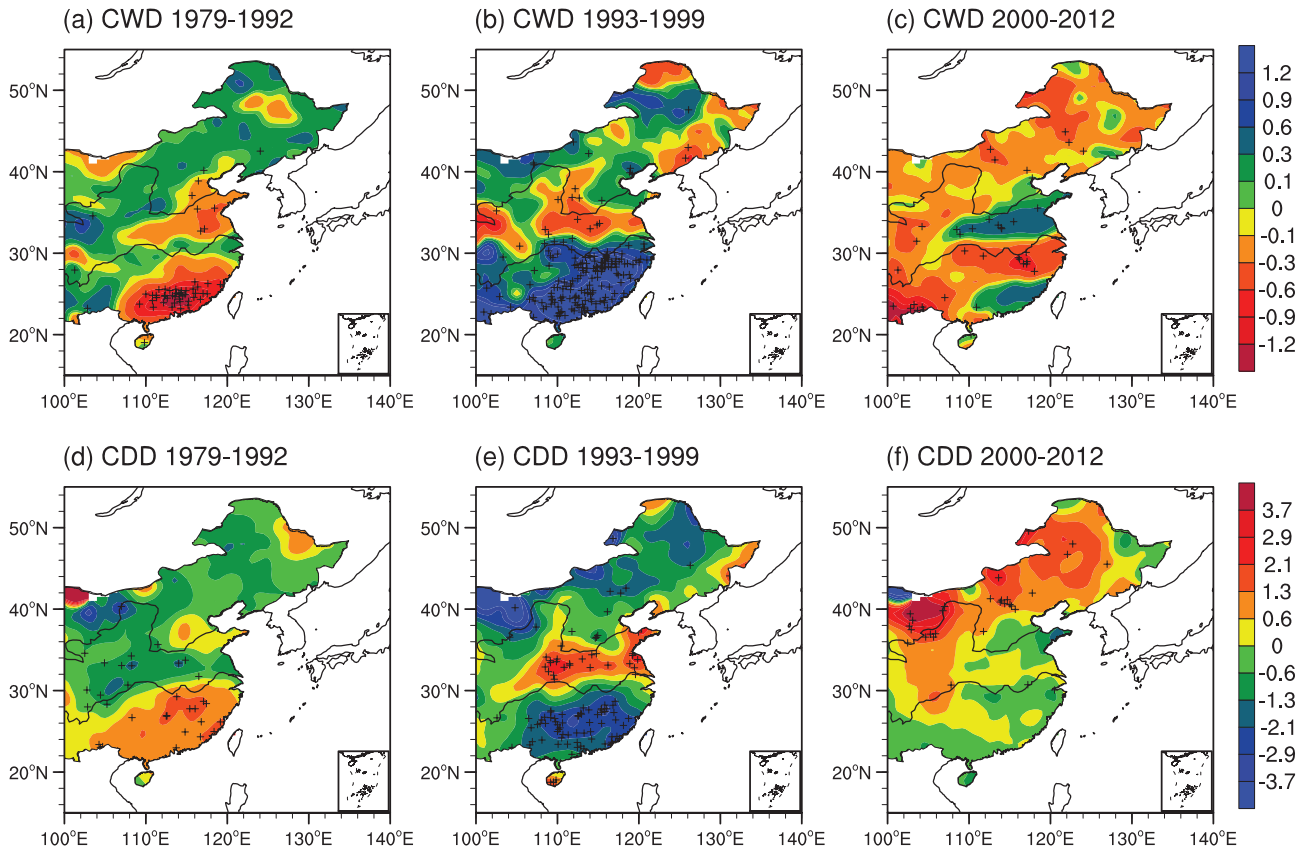

Figure 5. Anomalies of maximum number of consecutive wet days (CWD, top panel) (days year^{-1}) and consecutive dry days (CDD, bottom panel) (days year^{-1}) during summer for the three sub-periods: (a) 1979–1992, (b) 1993–1999 and (c) 2000–2012, relative to the 1979–2012 average. The black crosses indicate the CWD or CDD exceeding the 90% significance level based on the Student's *t*-test.

anomalies are high with values of 0.78, 0.76 and 0.77 in the three sub-periods, respectively.

In order to reveal further the feature of extreme precipitation, Figure 5 shows the anomalies of CWD and CDD for the three sub-periods as an indication of persistent precipitation and drought in China. Compared to Figure 3, the patterns of CWD and precipitation anomalies are similar for all three sub-periods, with pattern correlation coefficients above 0.5 in each sub-period. In period I, both CWD and precipitation show positive anomalies in Northeast China and Sichuan Basin. During period II, positive precipitation and CWD anomalies almost occur over the entire East China except the central part and part of Northeast China (Figure 5(b)). In the last period, both positive precipitation anomalies and CWD anomalies are located in Huang-Huai River and South China (Figure 5(c)). As expected, the CDD anomalies are almost negatively correlated ($R_{\mathrm{I}} = -0.52$ and $R_{\mathrm{II}} = -0.49$) with the precipitation anomalies in the first two sub-periods, with a few exceptions. For example, the positive CDD anomaly occupies a smaller coverage than the negative precipitation anomalies over Huang-huai River in period I (Figure 5(d)), and the negative CDD anomaly does not cover the whole Central China in period II (Figure 5(e)). In period III, CDD anomalies over MLYRB and Southwest China where negative precipitation anomalies occur are negative (Figure 5(f)).

The spatial distributions of HY-INT, dry spell (DSL) and INT averaged for the three sub-periods are presented in Figure 6. The spatial correlation coefficients between HY-INT and DSL are higher than that between HY-INT and INT in three sub-periods, more than 0.6, shown in top right of Figure 6(d)–(f). In period I, high HY-INT values mainly occur in and to the south of the Yangtze River Basin, which indicate a high risk of intense precipitation and/or long drought events there. This may be due to some dry events in South China during this period (Figure 6(d)). In period II, the high risk of extreme events in North China may be associated with the increase of wet events. In period III, except for the middle-lower Yellow River Basin, most regions suffer a high risk of extreme events. The high HY-INT over Northeast China may be caused mainly by dry events, while the HY-INT over South China may be due to relatively wet conditions.

To reveal the interannual and interdecadal variations of regional precipitation and extreme events, the region of eastern China is divided into five climatic sub-regions (as shown in Figure 2(a)): Northeast China (NEC), North China (NC), Huang-huai River (HHR), middle-lower Yangtze River (MLYR) and South China (SC), based on the location of the regime shift detection method for shift years around 1992/1993 (Figure 2(b)) and 1999/2000 (Figure 2(c)). The annual variations of mean precipitation and extreme indices averaged over the five sub-regions

© 2015 Royal Meteorological Society

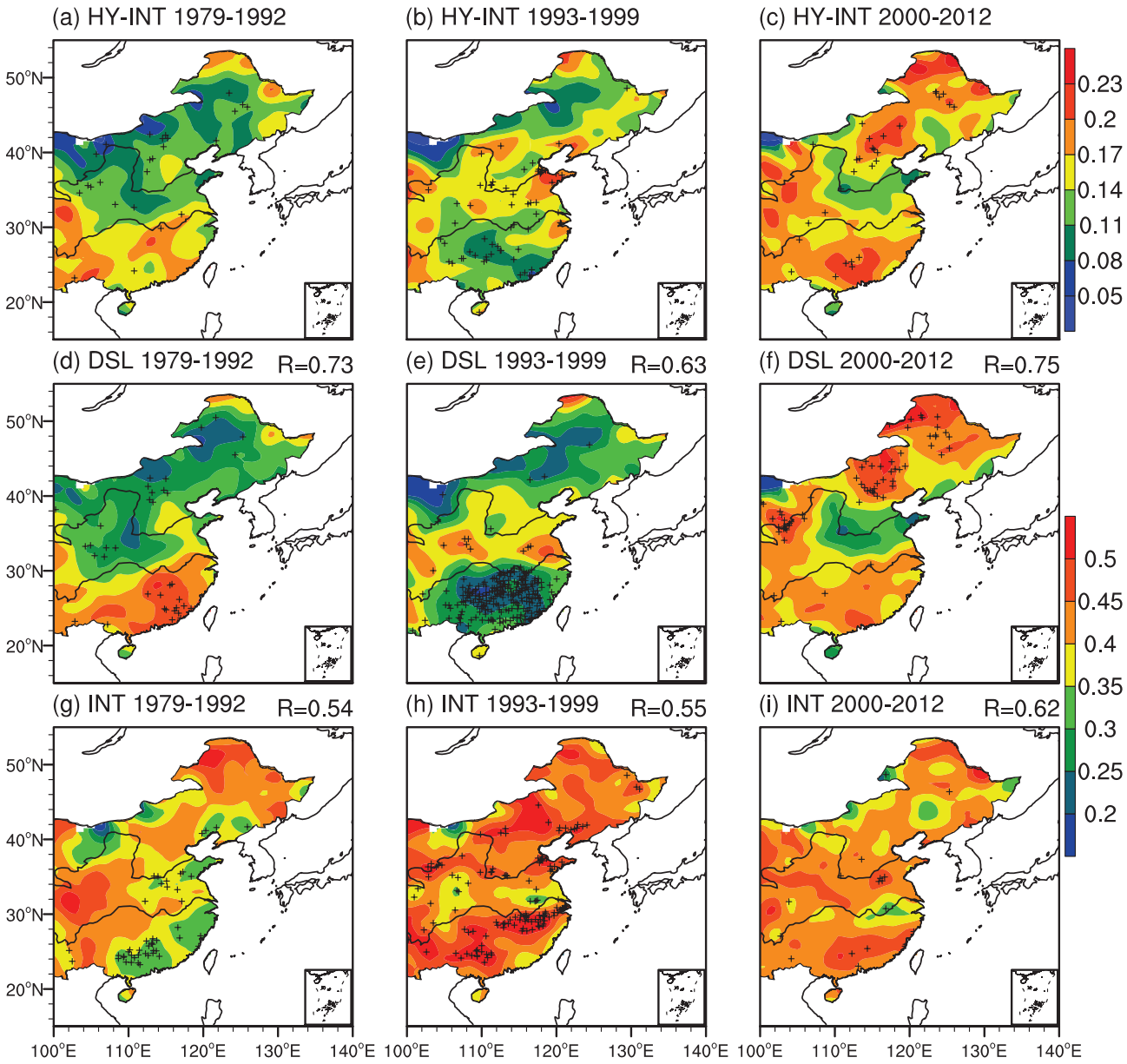

Figure 6. Summer hydroclimatic intensity (HY-INT, a–c), the mean number of consecutive dry days during each dry spell (DSL, d–f) and the mean precipitation intensity during wet days (INT, g–i) averaged for the three sub-periods, respectively. The stations with the black cross are statistically significant exceeding 90% significance level based on the Student's *t*-test. The spatial correlation coefficients between HY-INT and DSL (INT) are shown at the top right of each panel (d–i).

are shown in Figure 7. In general, the annual variations of mean precipitation and R95p (or CWD) are consistent with each other and negatively correlated with that of CDD (except in MLYR) to some extent in all five regions, indicating a coherent relationship among mean precipitation, R95p, CWD and CDD. In particular, the correlation coefficients between mean precipitation and R95p (or CWD) in each sub-region is higher than 0.89 (0.74). In addition, interannual and interdecadal variations of mean precipitation and the extreme indices are obvious in these sub-regions, but the shift years are different, which result in different precipitation and extreme precipitation patterns in China. In NEC (HHR), the abrupt decrease (increase) in mean precipitation, R95p and CWD all occur around 1999/2000, while the significant increase (decrease) in CDD is found around 1999. In NC, the variation amplitudes of mean precipitation, R95p and CWD increase during 1993–1999. In MLYR, mean precipitation, R95p and CWD exhibit weak interannual upward trend after 1993 and significant decrease after 1999. Although the relationship between mean precipitation and CDD is poor, the shift years of CDD are consistent with that of other three extreme indices. And in region SC, mean precipitation, R95p and CWD increase substantially after 1993, while CDD decreases. The time series of mean precipitation and these three indices in NEC, HHR and MLYR reflect the second shift year, and in SC, they reflect the first shift year. In region NC, both the first and the

© 2015 Royal Meteorological Society

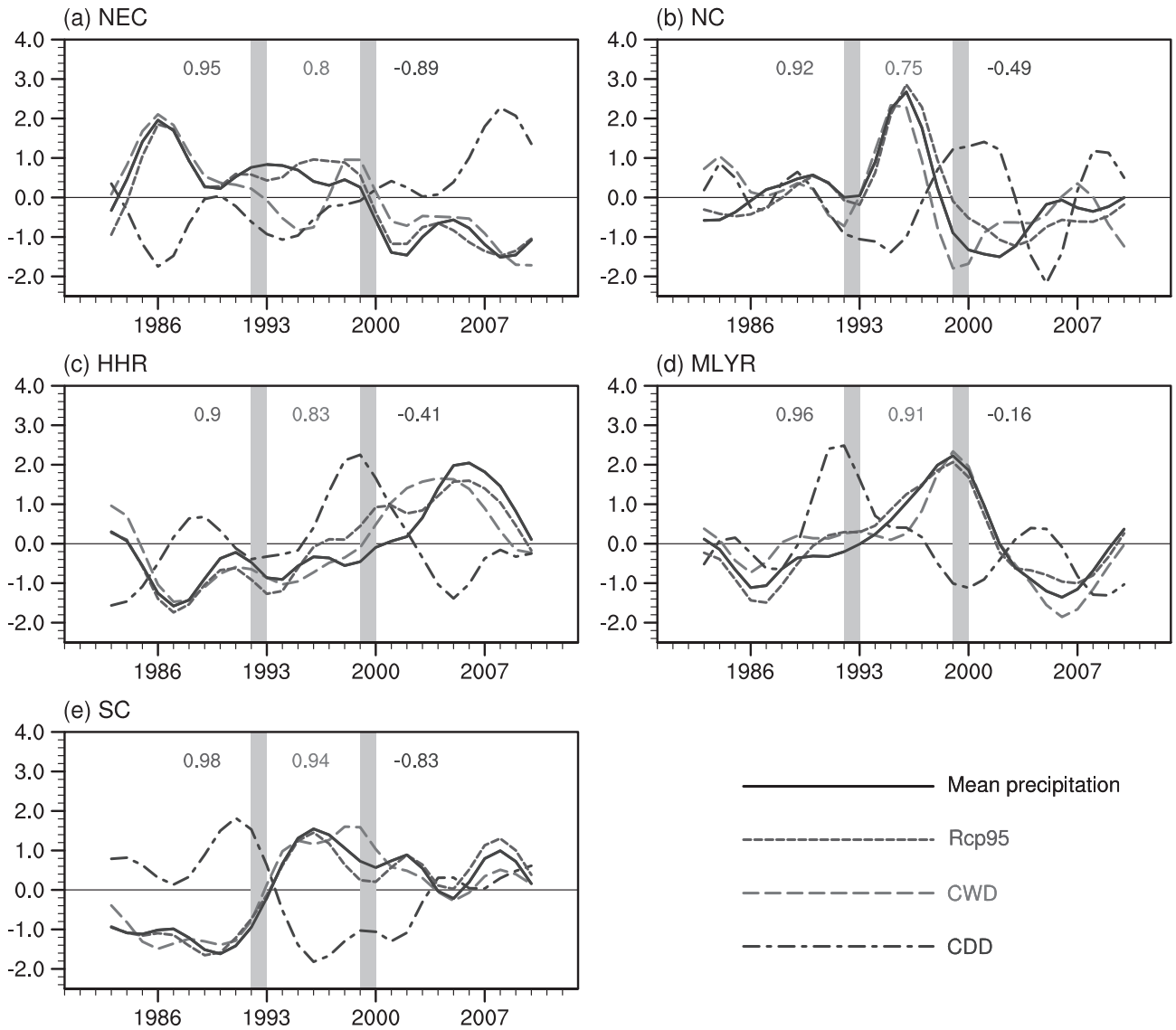

Figure 7. The standardized time series (with 7-year low-pass-filtered) of the mean precipitation, the number of days with daily rainfall exceeding 95th percentile precipitation (R95p), the maximum number of consecutive wet days (CWD) and the maximum number of consecutive dry days (CDD) averaged over NEC (a), NC (b), HHR (c), MLYR (d) and SC (e), respectively, during summer. The correlation coefficients between mean precipitation and three extreme indices are shown at each panel with the colours corresponding to the line colours of the three indices.

second shift years could be detected there. The analysis of regional precipitation and extreme events further confirms the division of the sub-periods adopted above.

To attribute the variations of HY-INT and investigate whether HY-INT has the same shift years as the precipitation anomaly patterns, we calculate the regional averaged number of consecutive dry days during each dry spell (DSL) and the precipitation intensity during wet days (INT) (Figure 8). The result shows that the time series of HY-INT and DSL are correlated to each other, especially in the sub-regions of NEC ($R = 0.96$), NC ($R = 0.93$) and HHR ($R = 0.89$), which means that DSL dominates the changes of HY-INT in eastern China. Although the spatial patterns of HY-INT in the three sub-periods are different from that of precipitation and extreme events, the shift years of them are close to each other in individual regions. As shown in Figure 8(a), NEC experiences a weak rising trend, especially after 1999. In HHR, just the second shift (the shift year around 1999/2000) could be found. In the other three regions, both the first (the shift year around 1992/1993) and the second shifts could be detected.

Figure 9 illustrates the four extreme indices over the five sub-regions of East China during the three sub-periods. The north-to-south variations of R95p over the area north (south) to Huai River in the first and third periods are similar to that of CWD, both showing a decline (increase) in R95p and CWD from NEC to HHR in the first period and from MLYR to SC in the third period. Both CDD and HY-INT show anti-phase variations with the R95p and CWD mentioned above except for the CDD over HHR in period I. In period II, the north-to-south variations of HY-INT over East China are similar to that of CDD, indicating that the risk of extreme event during this period is

© 2015 Royal Meteorological Society

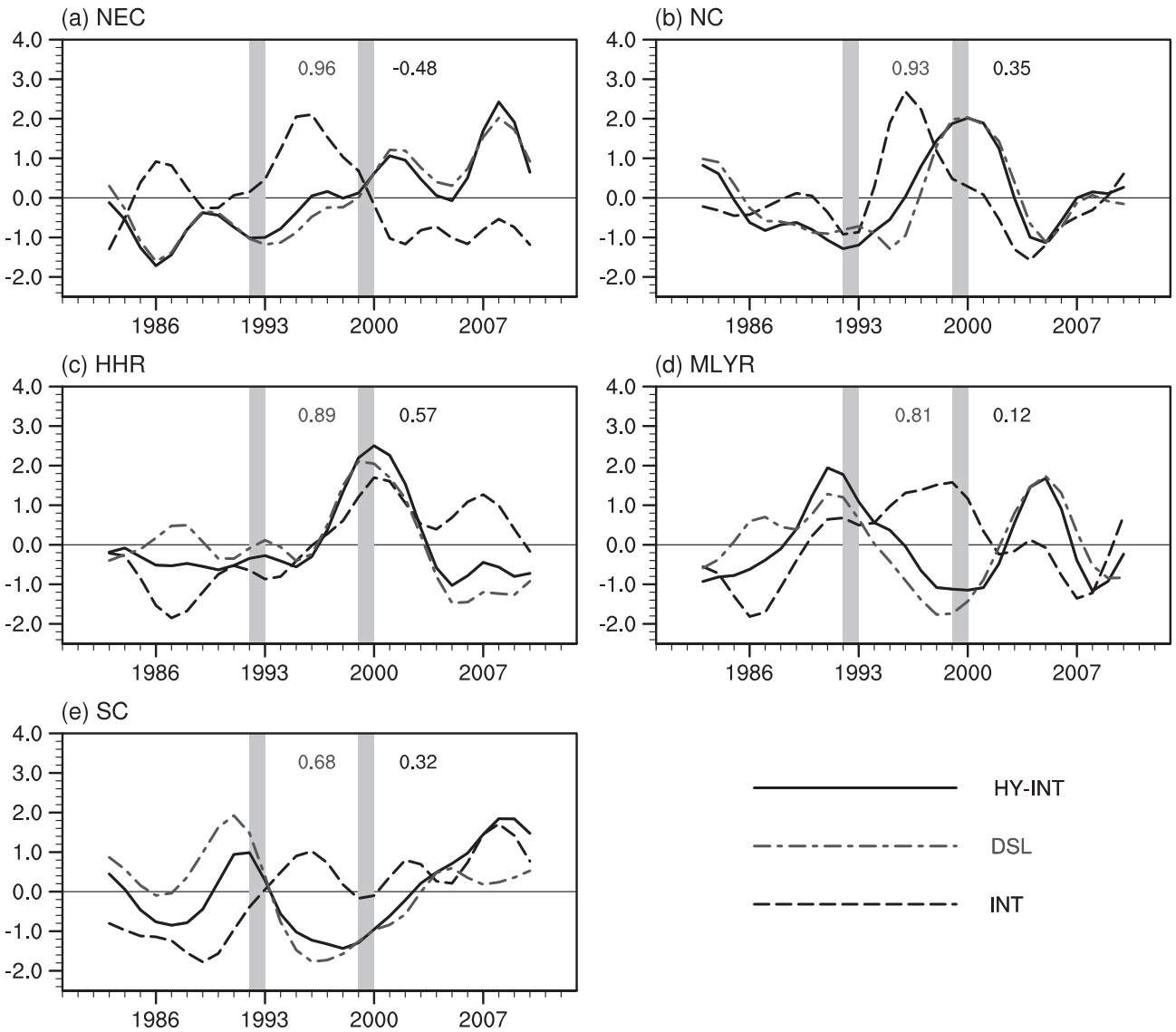

Figure 8. The standardized time series (with 7-year low-pass-filtered) of the hydroclimatic intensity (HY-INT), and the mean number of consecutive dry days during each dry spell (DSL), and the mean precipitation intensity during wet days (INT) averaged over NEC (a), NC (b), HHR (c), MLYR (d) and SC (e), respectively, during summer. The correlation coefficients between HY-INT and DSL (INT) are shown at the top middle (right) of each panel.

mostly related to drought. From NEC to HHR, the variations of R95p are consistent with that of CWD. However, the disagreement in variations between R95p and CWD is detected from MLYR to SC.

3.3. Possible reasons of precipitation anomaly variations

The EASM index proposed by Wu and Ni (1997) is used for the analysis of interdecadal variation. This index is defined as the meridional wind anomaly at 850 hPa averaged over East Asia (20°–30°N, 110°–130°E). Figure 10 shows the time series of EASM index based on three reanalysis data sets for 1979–2012. The time series, showing good agreement among the three reanalysis data sets, have two robust shifts in 1992/1993 and 1999/2000. These two shifts notably coincide with the changes in precipitation patterns, suggesting that the interannual and interdecadal variation of precipitation anomalies and extreme events in China are highly correlated with that of EASM. In addition, the strength of EASM also influences the position of the rainband. In period I, the strength of EASM is weak, resulting in more precipitation over the northern MLYR. In period II, the stronger EASM is accompanied by a northward shift of the rainband to North China, as the Meiyu front propagates further north. In period III, the rainband retreats to Huang-huai River as the strength of EASM becomes weaker initially, but strengthens in the middle of this period.

In general, precipitation is driven by the convergence of moisture fluxes (e.g. Lu and Kim, 2004; Huang *et al.*, 2013). Figure 11 depicts the climatological JJA mean moisture flux for the whole time period, the anomalies of moisture flux and divergence averaged in the three sub-periods. The anomalies of moisture transport and

© 2015 Royal Meteorological Society

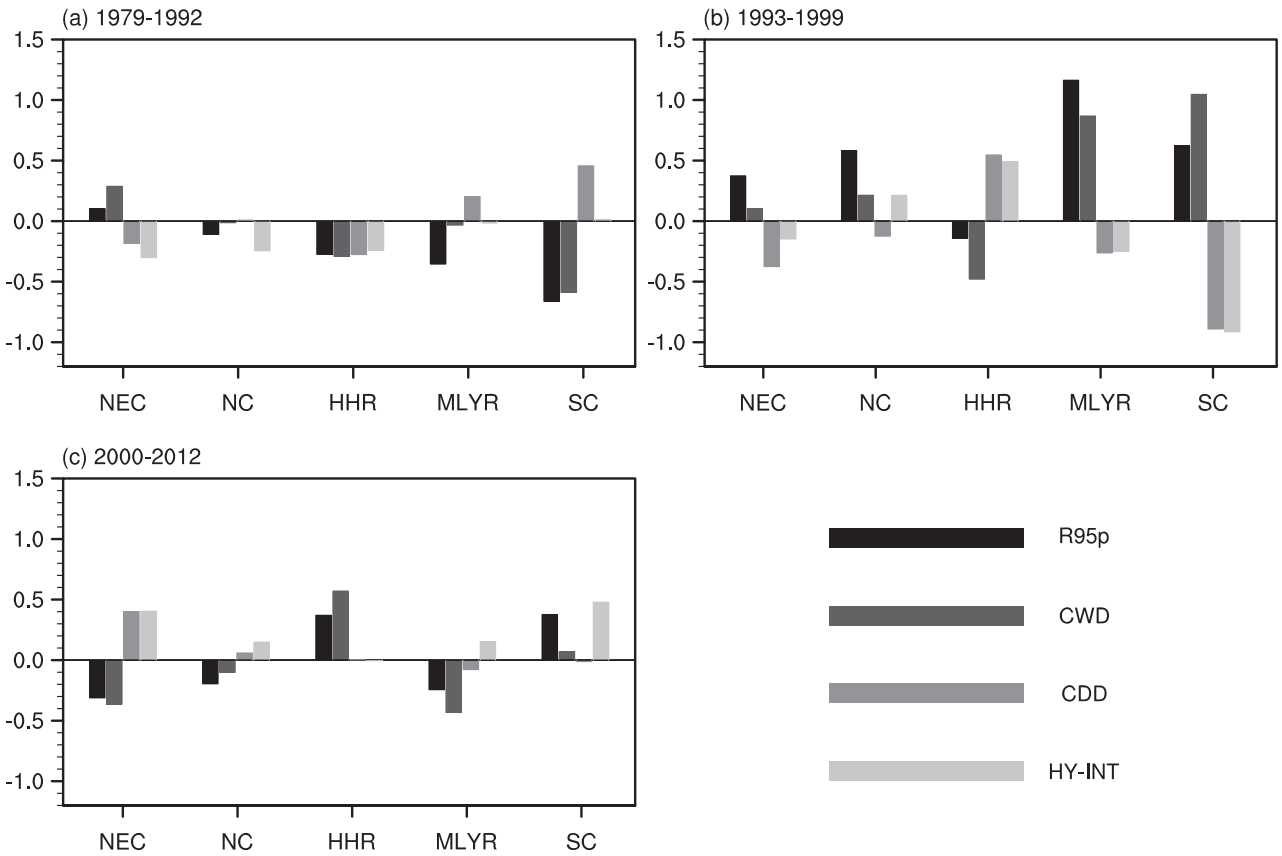

Figure 9. The regional averaged values of four indices: the number of days with daily precipitation exceeding 95th percentile precipitation (R95p), the maximum number of consecutive wet days (CWD), the maximum number of consecutive dry days (CDD) and the hydroclimatic intensity (HY-INT) in three sub-periods during summer.

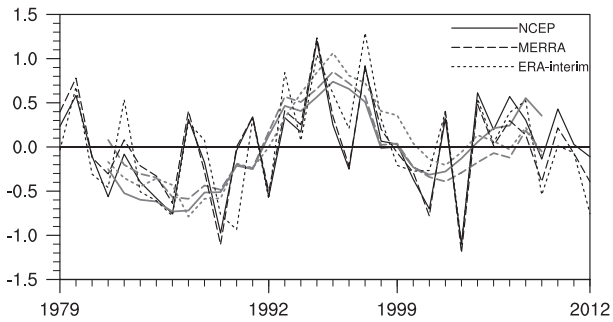

Figure 10. The 34-year (1979–2012) time series of EASM index based on three reanalysis data sets. The three grey lines are the 7-year running mean corresponding to the black lines, respectively.

divergence are spatially consistent with the precipitation anomalies shown in Figure 3(a), especially to the south of the Huai River. In the low-latitudes monsoon region, Indian monsoon transports the strong moisture from Bay of Bengal to Southeast China (Figure 11(a)), which is the main source of summer monsoon precipitation in China. Another moisture source is the moisture transport by the East Asian monsoon circulation from Western Pacific to Southeast China (Simmonds *et al.*, 1999; Ding and Chan, 2005; Zhou and Yu, 2005). In period I, there is an absence of moisture transport from West Pacific to East China. Moreover, the cyclonic circulation anomaly over South China Sea suppresses southwesterly moisture transport (Figure 11(a)) to South China, which results in less precipitation over there (Figure 11(b)). In period II, significant southwesterly moisture flux anomalies transport more moisture from the tropical western Pacific to East Asia, resulting in persistent higher moisture content over South China (Figure 11(c)). In period III, moisture transport that originates from the subtropical western Pacific forms a cyclonic anomaly over Southeast China, bringing positive moisture transport flux divergence anomalies in the MLYRB and Southwest China but negative anomalies in South China (Figure 11(d)).

In the mid-latitudes, the moisture transport flux is dominated by the westerlies and is weaker than the low-latitudes. In period II, the Central China is covered by moisture transport flux divergence anomalies (Figure 11(c)). In period I, a large cyclonic southwesterly convergence anomaly over Northeast China brings more moisture there (Figure 11(b)), while an anticyclonic anomaly below the Lake Baikal leads to less moisture over Northeast China in period III (Figure 11(d)). In addition, the spatial distribution of moisture transport flux in period III is nearly reversed compared to that of period I, which may generate the reversed precipitation anomaly pattern. Therefore, more analysis of the moisture transport is important to understand the underlying mechanisms that govern precipitation anomaly patterns.

© 2015 Royal Meteorological Society

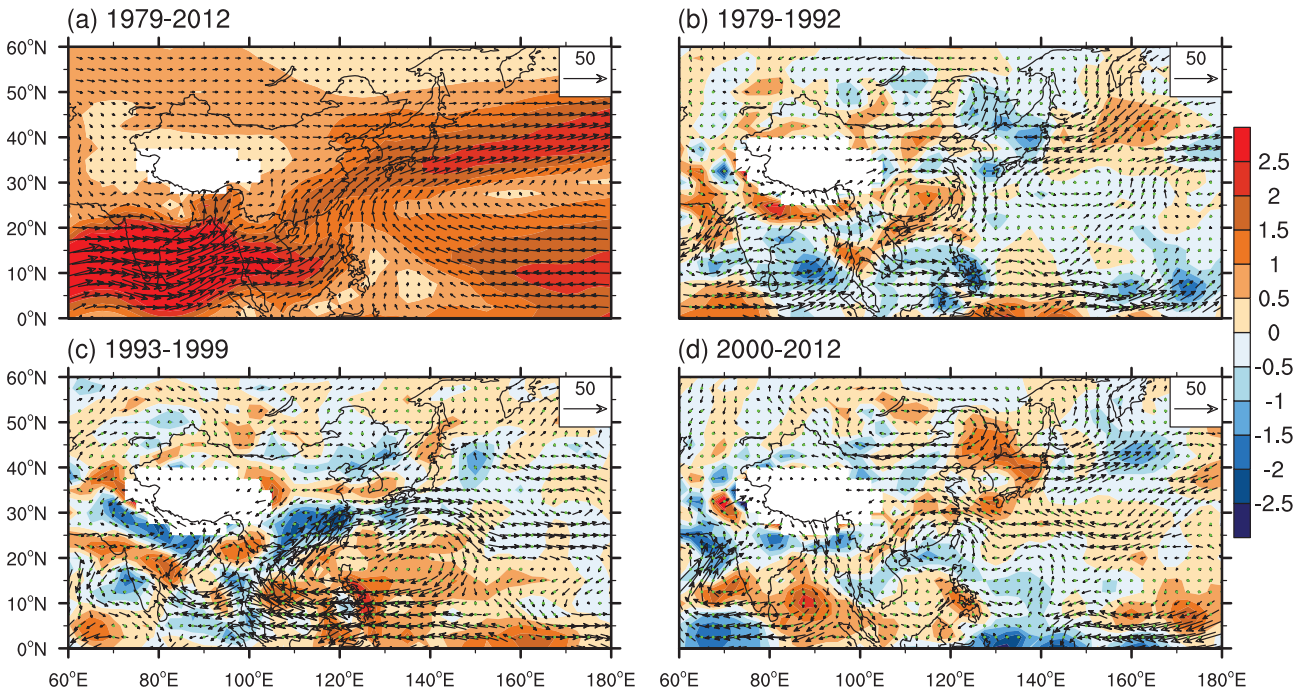

Figure 11. (a) Vertically integrated (1000–300 hPa) JJA mean moisture flux (vectors in 100 kg m^{-1} s^{-1}) for 1979–2012. The shading indicates the magnitude of the moisture flux vector. Anomalies of vertically integrated (1000–300 hPa) JJA moisture flux (vectors in kg m^{-1} s^{-1}) and divergence (shading in 10^{-5} kg m^{-2} s^{-1}) averaged for the three sub-periods: (b) 1979–1992, (c) 1993–1999 and (d) 2000–2012, relative to 1979–2012. The green dots indicate the moisture flux divergence exceeding the 90% significance level based on the Student's *t*-test.

As a key component of the EASM system, the West Pacific Subtropical High (WPSH) has a great influence on the climate of China, with its intensity and location closely associated with summer precipitation (Tao and Chen, 1987; Huang and Wu, 1989; Hu, 1997; He *et al.*, 2001). To analyse the characteristics of WPSH, two indices including intensity and western ridge point are adopted following the definition given by Beijing Climate Center. The intensity index is defined as the accumulated value of the 500 hPa geopotential height anomaly (relative to 587 geopotential decameter) in the grids with the height larger than 588 gpdm in region (10°–the North Pole, 110°–180°E). The western ridge point index is the most west longitude of the contour 588 gpdm from 90° to 180°E. After comparing the time series of two indices, we find that both the intensity and the western ridge point show remarkable interannual and interdecadal variations during the entire period as shown in Figure 12(a) and (b). The interannual and interdecadal variation of the western ridge point index is consistent with that of precipitation patterns showing the shift years in 1992/1993 and 1998/1999. The interannual and interdecadal regime shifts of the intensity index are generally similar with that of precipitation patterns in China, although its shift years are a little different from those of precipitation. The disagreements are observed in the early 1990s, mid-1990s and early 2000s. From the perspective of large-scale atmospheric circulation, WPSH influences on the precipitation patterns in East China through its effect on the anomalies of moisture transport path. The WPSH is relatively stronger and extends more westward after 1992/1993. In the meantime,

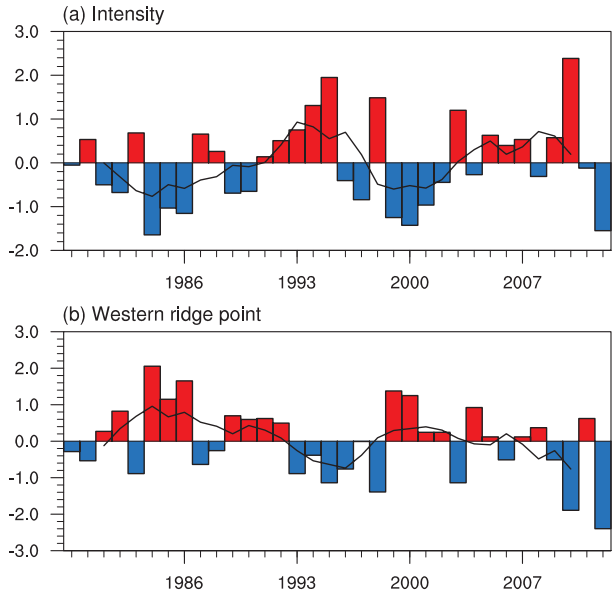

Figure 12. The standardized intensity, western ridge point index of the 500 hPa geopotential height, with the black lines indicating the 5-year running mean.

the circulation along the edge of WPSH transports more moisture from tropical West Pacific to the edge of East China, which increases southwesterly moisture transport to MLYRB and Southeast China. Since 1999/2000, the WPSH becomes weaker and moves towards eastward, and the southwesterly moisture transport is suppressed. Similar result was proposed by Gong and Ho (2002) and Hu (1997), who showed that the abrupt change of summer

© 2015 Royal Meteorological Society

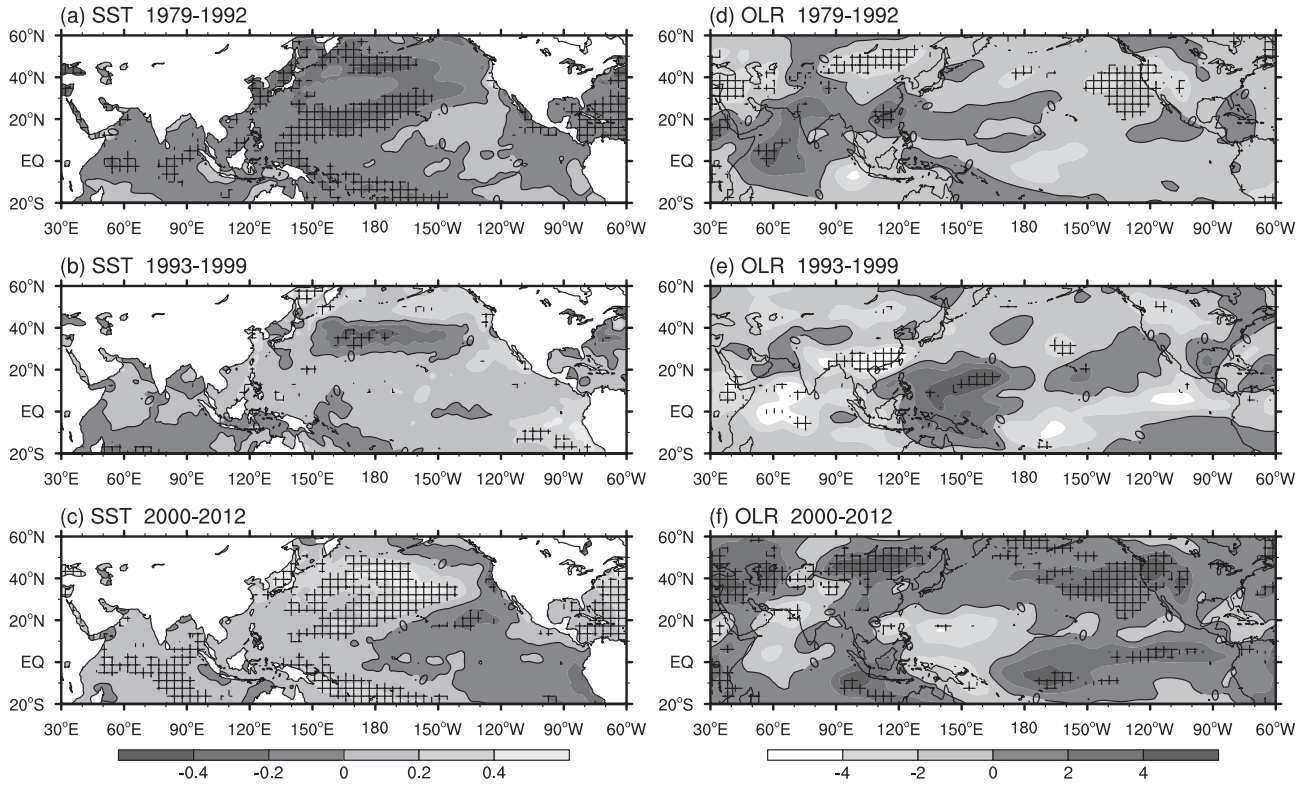

Figure 13. Anomalies of summer (a–c) SST (°C) and (d–f) OLR (W m^{-2}) averaged for the three sub-periods relative to 1979–2012. The black grids indicate the SST or OLR exceeding the 80% significance level based on the Student's *t*-test.

climate over East Asia and the change in summer precipitation over Yangtze River Basin in the late 1970s were both related to the intensification and southwestward extension of the WPSH. Our analysis confirms that the changes in precipitation anomaly patterns in China are closely related to the WPSH's intensity and position.

Having demonstrated that the summer precipitation in China is largely controlled by EASM through moisture transport by large-scale circulation features, it is important to understand factors that influence EASM on interannual and interdecadal time scales. Wu and Wang (2002) showed that the significant transition of the EASM in the late 1970s is correlated strongly with the climate change in the tropical Pacific. The warming in the tropical Indian Ocean also plays an important role in inducing the anticyclone anomaly over the West Pacific (Wu *et al.*, 2009). The changes in the intensity and location of convection anomaly over the West Pacific contribute most to the change in the ENSO-related East Asian summer circulation anomaly, through the teleconnection pattern, i.e. 'Pacific–Japan (PJ) pattern' (Nitta, 1987; Kosaka and Nakamura, 2006) or 'East Asia-Pacific pattern' (Huang, 1992). Sun and Wang (2014) systematically analysed the climate in tropical Pacific and Indian Ocean and its linkage with the moisture transport anomaly over the East Asian. They suggested that the warming in the SST over the Maritime Continent would strengthen the convective anomaly there, which may induce a meridional wave train causing the descending and anticyclonic anomaly over the West Pacific and South China. Moreover, the anomalous ascending near the Maritime Continent and the anomalous descending over central-eastern tropical Pacific, with easterly anomaly at low level and westerly anomaly at upper level over western-central Pacific, may strengthen the Walker circulation.

This article mainly focuses on the relationship between the moisture transport anomaly over the East Asian and convection anomaly causing by the tropical Pacific and Indian Ocean. As shown in Figure 13(a)–(c), the changes in SST over some regions of tropical Pacific and Indian Ocean are significant in different sub-periods. The SST there is divided into three regimes: the tropical Indian, West Pacific and East Pacific, consistent with previous studies (e.g. Hu, 1997; Chang *et al.*, 2000). In period I, only the East Pacific is warming, while the other two regions are cooling. In period II, the tropical Indian and Pacific are all warming. In period III, the Indian and West Pacific are warming but the other region is cooling. The possible mechanism for the SST-EASM (moisture transport) relationship is the presence or absence of the deep convection associated with the SST anomaly (SSTA) that can lead to an anomaly of the Northwest Pacific anticyclone or cyclone, which is well recognized as the dominant mode of interannual variability of EASM (Wang *et al.*, 2008; Fan *et al.*, 2013). The deep convection inferred by the OLR anomaly shown in Figure 13(d)–(f) shows some clear correspondence with the SSTA in Figure 13(a)–(c), although large-scale circulation pattern has often been invoked to account for the relationship between deep convection and SST (Lau *et al.*, 1997). The enhanced

© 2015 Royal Meteorological Society

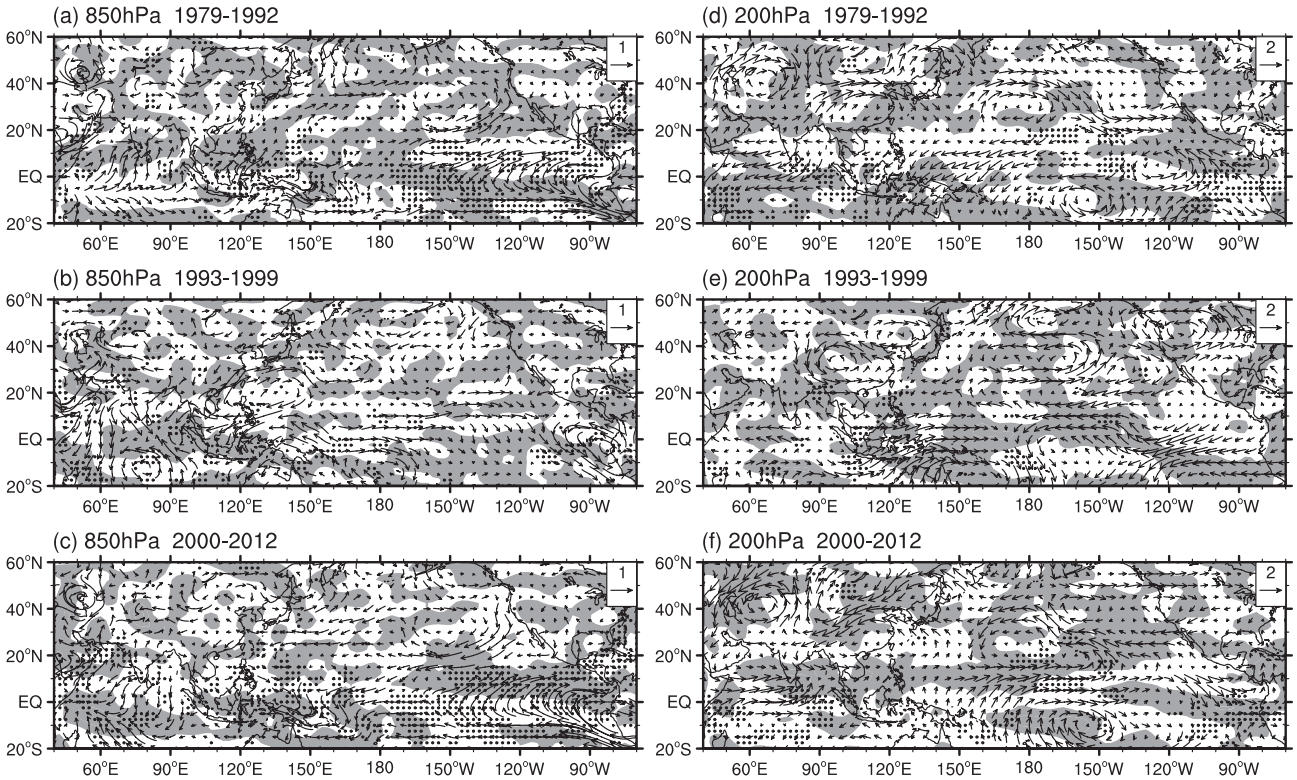

Figure 14. Anomalies of summer wind (vector), and its divergence (shading) at 850 hPa (a–c) and 200 hPa (d–f) for the three sub-periods relative to 1979–2012. The shading illustrates the areas of convergence anomalies. The dots indicate the wind divergence at 850 and 200 hPa exceeding the 90% significance level based on the Student's *t*-test.

convective activities with warm SST over East Pacific and Indian Ocean in period II produces low level convergence (Figure 14(b)) and upper level divergence (Figure 14(e)) over these two regions, which may cause the westerly (easterly) anomaly at low level and easterly (westerly) anomaly at upper level over the tropic Pacific (East Indian Ocean). With strong warm SSTAs over the East Pacific and the Indian Ocean (Figure 13(b)), deep convection induces an anomalous circulation with a subsiding branch over Northwest Pacific where an anticyclone forms (Figures 11(c) and 14(b)). In period III, the significant difference of SST between tropical West and East Pacific leads to the deep convection enhanced over the Northwest Pacific, which may induce the positive PJ pattern, i.e. the cyclonic anomaly over South China and Northwest Pacific and the anticyclonic anomaly to the south-east of Japan (Figures 11(d) and 14(c)). Compared to period III, the distribution of SSTA over tropical Ocean in period I shows the nearly reversed pattern. The suppressed convective activity with cold SST over West Pacific may induce the negative PJ pattern, corresponding to the anticyclonic anomaly over South China and Northwest Pacific and the cyclonic anomaly to the south-east of Japan (Figures 11(b) and 14(a)). The underlying mechanisms in this article, associated with the relationship between the anomalous convective activity over West Pacific and the circulation anomaly over the regions to its north, are consistent with previous findings (e.g. Nitta, 1989; Kosaka and Nakamura, 2006; Sun and Wang, 2014).

4. Discussion

We only investigate the mechanism associated with the mean precipitation anomalies, because R95p and CWD share the similar pattern to that of mean precipitation in many regions. However, in some regions, the variations of CDD are low correlated with that of mean precipitation, such as MLYR. The mechanism for it needs to be further studied in our future work.

5. Conclusions

In this study, the interannual and interdecadal variations of extreme precipitation are investigated using four extreme indices, from the perspective of occurrence frequency, persistence and the risk of occurrence, based on daily precipitation data at 2076 observational stations over East China from 1979 to 2012. The mechanisms associated with the changes in precipitation anomalies and extreme events were further studied using NCEP/NCAR reanalysis data sets. During the period 1979–2012, EOF-PC1 and -PC2 of summer total precipitation in East China show significant interdecadal variations and notable shifts around 1992/1993 and 1999/2000, respectively. The analysis of precipitation regime at individual stations confirms the variations of precipitation in East China given by EOF analysis. The whole period from 1979 to 2012 is then divided into three sub-periods for analysis

© 2015 Royal Meteorological Society

of interannual variations of precipitation anomalies and extreme events.

Generally, the spatial patterns of summer mean precipitation, R95p and CWD anomalies are consistent, but opposite to that of CDD anomalies to some extent during the three sub-periods. In period I, positive precipitation, R95p and CWD anomaly and negative CDD anomaly are observed over Northeast China, Sichuan Basin with a northeast to southwest orientation and northern part of MLYR, while the spatial patterns of precipitation anomalies and extreme events in period III are nearly opposite to that of period I. In period II, the precipitation and extreme indices exhibit a meridional structure and belt-like distribution with positive anomalies occurring over the area north to Yellow River and south of Yangtze River. The shift years of these three indices in East China are also the same as that of the EOF time series, indicating that the changes in extreme precipitation occurrence frequency and persistence in East China are consistent with the interannual and interdecadal variations of precipitation over East China. In addition, the opposite spatial patterns between CWD and CDD, as well as the opposite time series between them, complement the conclusion from the IPCC 5th Assessment Report (IPCC, 2013), i.e. an increase in the frequency of one extreme can be accompanied by a decline in the opposite extreme, such as the numbers of hot and cold days.

Using HY-INT as a combined index of precipitation intensity and DSL length, its spatial patterns is found to be different from the anomalies of precipitation patterns, but its time series have a positive correlation ($R > 0.67$) with DSL in East China. This suggests that dry events are the main contributor to the variation of HY-INT in East China in the past few decades.

Large-scale atmospheric features, especially the anomaly of East Asian monsoon system, play a key role in affecting precipitation and extreme events over East China. The 7-year running mean time series of EASM index show significant shifts in 1992/1993 and 1999/2000, with weak, strong and neutral intensity in the three sub-periods, respectively. Both the shift years and the intensity variations of EASM are consistent with the interannual and interdecadal variations of the precipitation patterns. Moreover, the spatial distributions of the precipitation and moisture convergence anomalies are consistent with each other in East China. Most notably, precipitation anomalies and extreme events in East China generally vary with the intensity and western ridge point of WPSH, which appear to be the two key factors affecting EASM precipitation in East China.

Lastly, the SST-EASM relationships were analysed for the three sub-periods. In periods I and III, the possible mechanism is that the convective activity over the West Pacific influences the circulation over South China and Northwest Pacific in the form of teleconnection. In period II, convective activity over the West Pacific forced by the SST in tropical Pacific and Indian Ocean plays an important role in the circulation anomaly over South China and Northwest Pacific.

Acknowledgements

This work was supported by the National Basic Research Program of China (973 Program, grant 2012CB955901) and the Jiangsu Collaborative Innovation Center for Climate Change. YQ, CZ and LRL were supported by the US Department of Energy Office of Science Biological and Environmental Research as part of the Regional and Global Climate Modeling Program. The Pacific Northwest National Laboratory is operated for DOE by Battelle Memorial Institute under contract DE-AC05-76RL01830.

References

Alexander LV, Zhang X, Peterson TC, Caesar J, Gleason B, Tank AMGK, Haylock M, Collins D, Trewin B, Rahimzadeh F, Tagipour A, Kumar KR, Revadekar J, Griffiths G, Vincent L, Stephenson DB, Burn J, Aguilar E, Brunet M, Taylor M, New M, Zhai P, Rusticucci M, Vazquez-Aguirre JL. 2006. Global observed changes in daily climate extremes of temperature and precipitation. *J. Geophys. Res.* **111**: D05109, doi: 10.1029/2005JD006290.

Chang C, Zhang Y, Li T. 2000. Interannual and interdecadal variations of the East Asian summer monsoon and tropical Pacific SSTs. Part I: roles of the subtropical ridge. *J. Clim.* **13**: 4310–4325.

Changnon SD. 2003. Measures of economic impacts of weather extremes. *Bull. Am. Meteorol. Soc.* **84**: 1231–1235, doi: 10.1175/bams-84-9-1231.

Chen Y, Chen XY, Ren GY. 2010. Variation of extreme precipitation over the Chinese large river basins. *Adv. Clim. Change Res.* **6**: 265–269.

Chen HP, Sun JQ, Fan K. 2012. Decadal features of heavy rainfall events in eastern China. *Acta Meteorol. Sin.* **26**: 289–303, doi: 10.1007/s13351-012-0303-0.

Dee DP, Uppala SM, Simmons AJ, Berrisford P, Poli P, Kobayashi S, Andrae U, Balmaseda MA, Balsamo G, Bauer P, Bechtold P, Beljaars ACM, van de Berg L, Bidlot J, Bormann N, Delsol C, Dragani R, Fuentes M, Geer AJ, Haimberger L, Healy SB, Hersbach H, Hólm EV, Isaksen L, Kållberg P, Köhler M, Matricardi M, McNally AP, Monge-Sanz BM, Morcrette J-J, Park B-K, Peubey C, de Rosnay P, Tavolato C, Thépaut J-N, Vitart F. 2011. The ERA-Interim reanalysis: configuration and performance of the data assimilation system. *Q. J. R. Meteorol. Soc.* **137**: 553–597, doi: 10.1002/qj.828.

Ding YH, Chan JCL. 2005. The East Asian summer monsoon: an overview. *Meteorol. Atmos. Phys.* **89**: 117–142.

Ding YH, Wang ZY, Sun Y. 2008. Inter-decadal variation of the summer precipitation in East China and its association with decreasing Asian summer monsoon. Part I: observed evidences. *Int. J. Climatol.* **28**: 1139–1161, doi: 10.1002/joc.1615.

Fan L, Shin S-I, Liu QY, Liu ZY. 2013. Relative importance of tropical SST anomalies in forcing East Asian summer monsoon circulation. *Geophys. Res. Lett.* **40**: 2471–2477, doi: 10.1002/grl.50494.

Giorgi F, Im E-S, Coppola E, Diffenbaugh NS, Gao XJ, Mariotti L, Shi Y. 2011. Higher hydroclimatic intensity with global warming. *J. Clim.* **24**: 5309–5324, doi: 10.1175/2011JCLI3979.1.

Gong DY, Ho CH. 2002. Shift in the summer rainfall over the Yangtze River valley in the late 1970s. *Geophys. Res. Lett.* **29**: 1436.

Guo Q, Cai J, Shao X. 2003. Interdecadal variability of East-Asia summer monsoon and its impact on the climate of China. *Acta Geogr. Sin.* **4**: 569–576.

He JH, Zhou B, Wen M, Li F. 2001. Vertical circulation structure, interannual variation features and variation mechanism of western Pacific subtropical high. *Adv. Atmos. Sci.* **18**: 497–510.

Hu ZZ. 1997. Interdecadal variability of summer climate over East Asia and its association with 500 hPa height and global sea surface temperature. *J. Geophys. Res.* **102**: 19403–19412.

Huang RH. 1992. The East Asia-Pacific pattern teleconnection of summer circulation and climate anomaly in East Asia. *Acta Geogr. Sin.* **6**: 25–36.

Huang RH, Wu YF. 1989. The influence of ENSO on the summer climate change in China and its mechanism. *Adv. Atmos. Sci.* **6**: 21–32.

Huang RH, Huang G, Wei ZG. 2004. Climate variations of the summer monsoon over China. In *East Asian Monsoon*, Chang CP (ed). World Scientific: Singapore.

© 2015 Royal Meteorological Society

Huang RH, Chen JL, Huang G. 2007. Characteristics and variations of the East Asian monsoon system and its impacts on climate disasters in China. *Adv. Atmos. Sci.* **24**: 993–1023.

Huang DQ, Zhu J, Kuang XY. 2011a. Decadal variation of different durations of continuous Meiyu precipitation and the possible cause. *Chin. Sci. Bull.* **56**: 424–431.

Huang RH, Chen JL, Liu Y. 2011b. Interdecadal variation of the leading modes of summertime precipitation anomalies over eastern China and its association with water vapor transport over East Asia (in Chinese). *Chin. J. Atmos. Sci.* **35**: 589–606, doi: 10.3878/j.issn.1006-9895.2011.04.01.

Huang RH, Liu Y, Feng T. 2013. Interdecadal change of summer precipitation over Eastern China around the late-1990s and associated circulation anomalies, internal dynamical causes. *Chin. Sci. Bull.* **58**: 1339–1349, doi: 10.1007/s11434-012-5545-9.

IPCC. 2013. *Climate Change 2013*. The Physical Science Basis. Contribution of Working Group I to the Fifth Assessment Report of the Intergovernmental Panel on Climate Change, Stocker TF, Qin DH, Plattner G-K, Tignor M, Allen S, Boschung J, Nauels A, Xia Y, Bex V, Midgley PM (eds). Cambridge University Press: Cambridge, UK and New York, NY.

Jiang DB, Wang HJ. 2005. Natural interdecadal weakening of East Asian summer monsoon in the late 20th century. *Chin. Sci. Bull.* **50**: 1923–1929, doi: 10.1360/982005-36.

Kalnay E, Kanamitsu M, Kistler R, Collins W, Deaven D, Gandin L, Iredell M, Saha S, White G, Wollen J, Zhu Y, Chelliah M, Ebisuzaki W, Higgins W, Janowiak J, Mo KC, Ropelewski C, Wang J, Leetmaa A, Reynolds R, Jenne R, Joseph D. 1996. The NCEP/NCAR 40 year reanalysis project. *Bull. Am. Meteorol. Soc.* **77**: 437–471.

Kosaka Y, Nakamura H. 2006. Structure and dynamics of the summertime Pacific-Japan (PJ) teleconnection pattern. *Q. J. R. Meteorol. Soc.* **132**: 2009–2030.

Kunkel KE, Pielke RA Jr, Changnon SA. 1999. Temporal fluctuations in weather and climate extremes that cause economic and human health impacts: a review. *Bull. Am. Meteorol. Soc.* **80**: 1077–1098.

Kwon MH, Jhun JG, Ha KJ. 2007. Decadal change in East Asian summer monsoon circulation in the mid-1990s. *Geophys. Res. Lett.* **34**: L21706, doi: 10.1029/2007gl031977.

Lau KM, Wu HT, Bony S. 1997. The role of large-scale atmospheric circulation in the relationship between tropical convection and sea surface temperature. *J. Clim.* **10**: 381–392.

Li YF, Leung LR. 2013. Potential impacts of the Arctic on interannual and interdecadal summer precipitation over China. *J. Clim.* **26**: 899–917, doi: 10.1175/jcli-d-12-00075.1.

Li ZX, He YQ, Wang PY, Theakstone WH, An WL, Wang XF, Lu A, Zhang W, Cao WH. 2012. Changes of daily climate extremes in southwestern China during 1961-2008. *Glob. Planet Change* **80–81**: 255–272.

Liebmann B, Smith CA. 1996. Description of a complete (interpolated) outgoing longwave radiation dataset. *Bull. Am. Meteorol. Soc.* **77**: 1275–1277.

Lu RY. 1999. Interdecadal variations of precipitations in various months of summer in North China. *Plateau Meteorol.* **18**: 519 (in Chinese).

Lu RY. 2003. Linear relationship between the interdecadal and interannual variabilities of North China rainfall in rainy season. *Chin. Sci. Bull.* **48**: 1040–1044.

Lu RY, Kim BJ. 2004. The climatological Rossby wave source over the STCZs in the summer Northern Hemisphere. *J. Meteorol. Soc. Jpn.* **82**: 657–669.

Moberg A, Jones PD, Lister D, Walther A, Brunet M, Jacobeit J, Alexander LV, Della-Marta PM, Luterbacher J, Yiou P, Chen D, Klein Tank AMG, Saladié O, Sigró J, Aguilar E, Alexandersson H, Almarza C, Auer I, Barriendos M, Bergert M, Bergström H, Böhm R, Butler J, Caesar J, Drebs A, Founda D, Gerstengarbe F-W, Micela G, Maugeri M, Österle H, Panzic K, Petrakis M, Srnec L, Tolasz R, Tuomenvirta H, Werner P, Linderholm H, Philipp A, Wanner H, Xoplaki E. 2006. Indices for daily temperature and precipitation extremes in Europe analyzed for the period 1901–2000. *J. Geophys. Res.* **111**: D22106, doi: 10.1029.2006JD007103.

Nitta T. 1987. Convective activities in the tropical western Pacific and their impacts on the Northern Hemisphere summer circulation. *J. Meteorol. Soc. Jpn.* **65**: 165–171.

Nitta T. 1989. Global features of the Pacific-Japan oscillation. *Meteorol. Atmos. Phys.* **41**: 5–12.

North GR, Bell TL, Cohalan RF. 1982. Sampling errors in estimation of empirical orthogonal functions. *Mon. Weather Rev.* **110**: 699–706.

Peterson TC, Folland C, Gruza G, Hogg W, Mokssit A, Plummer N. 2001. Report on the activities of the working group on climate change detection and related rapporteurs 1998-2001. Report WCDMP-47, WMO-TD 1071, World Meteorological Organization, Geneva, Switzerland.

Piao SL, Ciais P, Huang Y, Shen ZH, Peng SS, Li JS, Zhou LP, Liu HY, Ma YC, Ding YH, Friedlingstein P, Liu CZ, Tan K, Yu YQ, Zhang TY, Fang JY. 2010. The impacts of climate change on water resource and agriculture in China. *Nature* **467**: 43–51.

Qian Y, Leung LR. 2007. A long-term regional model simulation and observations of the hydroclimate in China. *J. Geophys. Res.* **112**: D14104, doi: 10.1029/2006JD008134.

Qian W, Lin X. 2005. Regional trends in recent precipitation indices in China. *Meteorol. Atmos. Phys.* **90**: 193–207, doi: 10.1007/s00703-004-0101-z.

Qian Y, Gong D, Fan J, Leung LR, Bennartz R, Chen D, Wang W. 2009. Heavy pollution suppresses light rain in China: observations and modeling. *J. Geophys. Res.* **114**: D00K02, doi: 10.1029/2008JD011575.

Rayner NA, Parker DE, Horton EB, Folland CK, Alexander LV, Rowell DP. 2003. Global analyses of sea surface temperature, sea ice, and night marine air temperature since the late nineteenth century. *J. Geophys. Res.* **108**: 4407, doi: 10.1029/2002JD002670.

Rienecker MM, Suarez MJ, Gelaro R, Todling R, Bacmeister J, Liu E, Bosilovich MG, Schubert SD, Takacs L, Kim GK, Bloom S, Chen J, Collins D, Conaty A, Silva AD, Gu W, Joiner J, Koster RD, Lucchesi R, Molod A, Owens T, Pawson S, Pegion P, Redder CR, Reichle R, Robertson FR, Ruddick AG, Sienkiewicz M, Woollen J. 2011. MERRA-NASA's modern-era retrospective analysis for research and applications. *J. Clim.* **24**(14): 3624–3648.

Rodionov S. 2004. A sequential algorithm for testing climate regime shifts. *Geophys. Res. Lett.* **31**: L09204, doi: 10.1029/2004GL019448.

Sánchez E, Gallardo C, Gaertner MA, Arribas A, Castro M. 2004. Future climate extreme events in the Mediterranean simulated by a regional climate model: a first approach. *Glob. Planet Change* **44**: 163–180.

Simmonds I, Bi D, Hope P. 1999. Atmospheric water vapor flux and its association with rainfall in China in summer. *J. Clim.* **12**: 1353–1367.

Sun B, Wang HJ. 2014. Inter-decadal transition of the leading mode of inter-annual variability of summer rainfall in East China and its associated atmospheric water vapor transport. *Clim. Dyn.* **44**: 2703–2722.

Tao S, Chen L. 1987. A review of recent research on the East Asian summer monsoon in China. In *Monsoon Meteorology*, Chang CP, Krishnamurti TN (eds). Oxford University Press: New York, NY, 60–92.

Trenberth KE, Dai A, Rasmussen R, Parsons DB. 2003. The changing character of precipitation. *Bull. Am. Meteorol. Soc.* **94**: 1205–1217.

Wang HJ. 2001. The weakening of the Asian monsoon circulation after the end of 1970's. *Adv. Atmos. Sci.* **18**: 376–386.

Wang Y, Yan ZW. 2009. Trends in seasonal precipitation over China during 1961–2007. *Atmos. Oceanic Sci. Lett.* **2**: 165–171.

Wang YQ, Zhou L. 2005. Observed trends in extreme precipitation events in China during 1961–2001 and the associated changes in large-scale circulation. *Geophys. Res. Lett.* **32**: L09707, doi: 10.1029/2005GL022574.

Wang B, Wu ZW, Li JP, Liu J, Chang CP, Ding YH, Wu GX. 2008. How to measure the strength of the East Asian summer monsoon? *J. Clim.* **17**: 4449–4462.

Wu AM, Ni YQ. 1997. The influence of Tibetan Plateau on the interannual variability of Asian monsoon. *Adv. Atmos. Sci.* **14**: 491–504.

Wu RG, Wang B. 2002. A contrast of the East Asian summer monsoon-ENSO relationship between 1962–77 and 1978–93. *J. Clim.* **15**: 3266–3279.

Wu B, Zhou TJ, Li T. 2009. Seasonally evolving dominant interannual variability modes of East Asian climate. *J. Clim.* **22**: 2992–3005, doi: 10.1175/2008JCLI2710.1.

Xu ZQ, Ke F, Wang HJ. 2015. Decadal variation of summer precipitation over China and associated atmospheric circulation after the late 1990s. *J. Clim.* **28**: 4086–4106.

Xue F. 2001. Interannual to interdecadal variation of East Asian summer monsoon and its association with the global atmospheric circulation and sea surface temperature. *Adv. Atmos. Sci.* **18**: 567–575.

Yao C, Yang S, Qian WH, Lin ZM. 2008. Regional summer precipitation events in Asia and their changes in the past decades. *J. Geophys. Res.* **113**: D17107.

You QL, Kang SC, Aguilar E, Pepin N, Flügel W-A, Yan YP, Xu YW, Zhang YJ, Huang J. 2011. Changes in daily climate extremes in China and their connection to the large scale atmospheric circulation during 1961–2003. *Clim. Dyn.* **36**: 2399–2417.

© 2015 Royal Meteorological Society

Yu RC, Wang B, Zhou TJ. 2004. Tropospheric cooling and summer monsoon weakening trend over East Asia. *Geophys. Res. Lett.* **31**: L22212, doi: 10.1029/2004GL021270.

Zhai P, Sun A, Ren FM, Liu XN, Gao B, Zhang Q. 1999. Changes of climate extremes in China. *Clim. Change* **42**: 203–218.

Zhai PM, Zhang XB, Wang H. 2005. Trends in total precipitation and frequency of daily precipitation extremes over China. *J. Clim.* **18**: 1096–1108.

Zhang DQ, Feng GL, Hu JG. 2008. Trend of extreme precipitation events over China in last 40 years. *Chin. Phys.* **17**: 736–742.

Zhang Q, Xu CY, Chen XH, Zhang ZX. 2011. Statistical behaviors of precipitation regimes in China and their links with atmospheric circulation 1960–2005. *Int. J. Climatol.* **31**: 1665–1678, doi: 10.1002/joc.2193.

Zhou TJ, Yu RC. 2005. Atmospheric water vapor transport associated with typical anomalous summer rainfall patterns in China. *J. Geophys. Res.* **110**: D08104, doi: 10.1029/2004JD005413.

Zhu YL, Wang H, Zhou W, Ma JH. 2010. Recent changes in the summer precipitation pattern in East China and the background circulation. *Clim. Dyn.* **36**: 1463–1473.

© 2015 Royal Meteorological Society